Estimation of CO concentration in high temperature PEM fuel cells using electrochemical impedance

Jensen, Hans-Christian Becker; Andreasen, Søren Juhl; Kær, Søren Knudsen; Schaltz, Erik

Published in:
Proceedings of the 5th International Conference on Fundamentals & Development of Fuel Cells

Publication date:
2013

Document Version
Early version, also known as pre-print

Estimation of CO concentration in high temperature PEM fuel cells using electrochemical impedance spectroscopy

Hans-Christian B. Jensen[a,*], Søren Juhl Andreasen[a], Søren Knudsen Kær[a], Erik Schaltz[a]

[a]*Aalborg University, Department of Energy Technology, Pontoppidanstræde 101, DK-9220, Aalborg, Denmark*

Abstract

Storing electrical energy is one of the main challenges for modern society grid systems containing increasing amounts of renewable energy from wind, solar and wave sources. Although batteries are excellent storage devices for electrical energy, their usage is often limited by a low energy density, a possible solution, an avoidance of the long recharging time is combining them with the use of fuel cells. Fuel cells continuously deliver electrical power as long as a proper fuel supply is maintained. The ideal fuel for fuel cells is hydrogen, which in it's pure for has high volumetric storage requirements. One of the solutions to this fuel storage problem is using liquid fuels such as methanol that through a chemical reformer converts the fuel into a hydrogen rich gas mixture. Methanol is a liquid fuel, which has low storage requirements and high temperature polymer electrolyte membrane (HTPEM) fuel cells can efficiently run on the reformed hydrogen rich gas, although with reduced performance depending on the contaminants, such as CO, in the gas.

By estimating the amount of CO in the fuel cell, it could be possible to adjust the fuel cell system operating parameters to increase performance of the reformer and fuel cell stack. This work focus on the estimation of CO percentage in the hydrogen rich anode gas in a fuel cell, by combining signal processing ideas with impedance information of the fuel cell while it is running. The presented approach functions during in the normal operating range of an HTPEM fuel cell.

Keywords: HTPEM, Fuel cell, Methanol, Reforming, CO estimation

1. Introduction

There is a growing demand for new clean energy sources, a demand which is expected to increase significantly, especially as stricter laws on emissions, which are planned, are put into force. The goal of these restrictions point towards zero emission, so it is not surprising that there is also a rise in the need for alternative energy sources, which have zero emission. Fuel cells are one of these alternative energy sources Pehnt (2001), which are used more and more, due to their increasing reliability (Numbers are presented in Tian et al. (2010)) and cost effectiveness (Price development for Fuel Cells are illustrated in DOE (2011)).

The state of the art method in signal processing methods regarding fuel cells is done with the impedance spectrum (There are articles on PAFC Choudhury and Rengaswamy (2006) and PEMFC Merida et al. (2006) Fuel Cells. Some combine fault diagnosis with state of health monitoring Fouquet et al. (2006), which is the area of focus in Gebregergis et al. (2010).). The presented methods so far are not able to do this during operation and require the fuel cell to be disconnected from the electrical load / grid during the test.

Efforts have been made in increasing operating temperatures of PEM fuel cells to minimize water management problems, increase fuel poisoning tolerances and decrease system complexity Zhang et al. (2006); Li et al. (2009). In the field of HTPEM fuel cells there is a growing interest in methanol reformers Avgouropoulos et al. (2009); Kolb et al. (2012); Jensen et al. (2007); Andreasen et al. (2008), as this gives the possibility to run on something other than pure

*Corresponding author. Tel.: +45 9940 9267; fax: +45 9815 1411
Email address: hcj@et.aau.dk (Hans-Christian B. Jensen)

hydrogen, which is proving to be one of the important factors in the full roll-out of fuel cells in commercial products. Hydrogen has high volumetric demands when it comes to storage and refueling and these are the interest of several companies researching into refueling stations http://www.hydrogen.energy.gov/pdfs/review10/st001_ahluwalia_2010_o_web.pdf (2010); http://www.fuelcells.org/info/charts/h2fuelingstations.pdf (2012). Methanol has the advantage of being a liquid fuel, but the challenge is to reform it into a hydrogen rich gas before entering the fuel cell, and the resulting fuel cell performance is highly dependent on the quality of the output reformer gas. One of the most important parameter is the CO % content, so an estimation of the CO contents is of interest for better control of the reforming process and thereby eventually also of the fuel cell system.

The fuel cell MEA used in this study is a Celtec-P2100 membrane produced by BASF with an active cell area of 45[cm^2]. Further information about the MEA are presented in BASF (2011b) and BASF (2011a)

This article serves as a proof of concept, analyzing the possibilities of using a signal processing based approach to obtain an estimate for the CO percentage contained in the fuel cell anode gas. This method uses a single frequency in the impedance spectrum to estimate the CO, which results in a fast and simple prediction of the CO concentration, compared to using the entire frequency sweep normally done in impedance spectroscopy. Since the method is signal based it requires excitation of the system through an input signal, but this signal can be introduced during normal operation, so the system can continue operation during CO estimation.

2. Nomenclature

A_{MEA}	Area of the MEA of a single cell [cm^2]
FC	fuel cell
$i_{cell}(t)$	Cell current [A]
MEA	Membrane electrode assembly
PEMFC	PEM Fuel Cell
$T_{cell}(t)$	Stack temperature [$^\circ C$]
$V_{cell}(t)$	Voltage produced by a single cell [V]
$Z_{Re}(t)$	Real part of impedance, which is the resistance [$\Omega\, cm^2$]
$Z_{Im}(t)$	Imaginary part of impedance, which is the reactance[$\Omega\, cm^2$]

2.1. Electrochemical Impedance Spectroscopy

Electrochemical impedance spectroscopy (EIS) is a well known characterisation method for electrochemical devices, and have been studied by several authors for use a characterisation tool for fuel cells both within modelling and state-of-health monitoring Yuan et al. (2007); Andreasen et al. (2011). The typical use of EIS with fuel cells involves super positioning a small amplitude sine wave signal to the DC current (galvanostatic measurement) or voltage (potentiostatic measurement) drawn from the fuel cell. Figure 1 shows the polarisation curve of a given fuel cell, illustrating that drawing a sinewave shaped current results in a voltage response also exhibiting sinusoidal behaviour, although with a different amplitude and phase depending on the different internal states of the fuel cell under test. In order to get pure sine wave behaviour the measurements typically need to be conducted at the linear area of the polarisation curve otherwise the resulting voltage response on a galvanostatic measurement will not yield a true sine wave output. For this reason the superimposed signals also need to be small in amplitude to avoid entering nonlinear regions of the polarisation curve.

Using signals with varying frequencies, the impedance of the fuel cell under test can be calculated by extracting the amplitudes and phase shifts of the current and voltage.

Using the extracted amplitudes (A_U and A_I) and phase shift (ϕ), the real (α) and imaginary part (β) of impedance $Z_{FC} = \alpha + j \cdot \beta$ can be calculated using equation 1 and 2 respectively.

$$\alpha = Re\left(\frac{A_U}{A_I}(cos(\phi) + jsin(\phi))\right) = \frac{A_U}{A_I}(cos(\phi)) \tag{1}$$

$$\beta = Im\left(\frac{A_U}{A_I}(cos(\phi) + jsin(\phi))\right) = \frac{A_U}{A_I}(sin(\phi)) \tag{2}$$

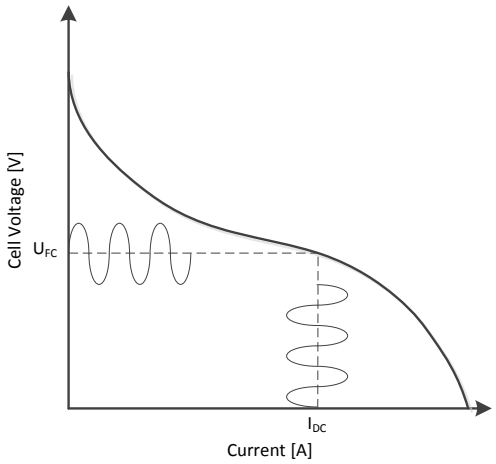

Figure 1: Graph showing how super positioning a small amplitude current sine wave results in sine wave voltage response.

This impedance describes the overall electrical behaviour of the fuel cell, a behaviour governed by all the different chemical and electrochemical processes occurring, diffusion of gasses and resistances in the different layers of the fuel cell. The impedance can be evaluated looking at magnitude and phase plot or as Nyquist plots, such as the one shown in figure 2, where the impedance of the HTPEM fuel cell under test is shown running on pure hydrogen at an anode stoichiometry of $\lambda_A = 1.3$, a cathode stoichiometry of $\lambda_C = 4$, a DC current of I_{DC} at different temperatures.

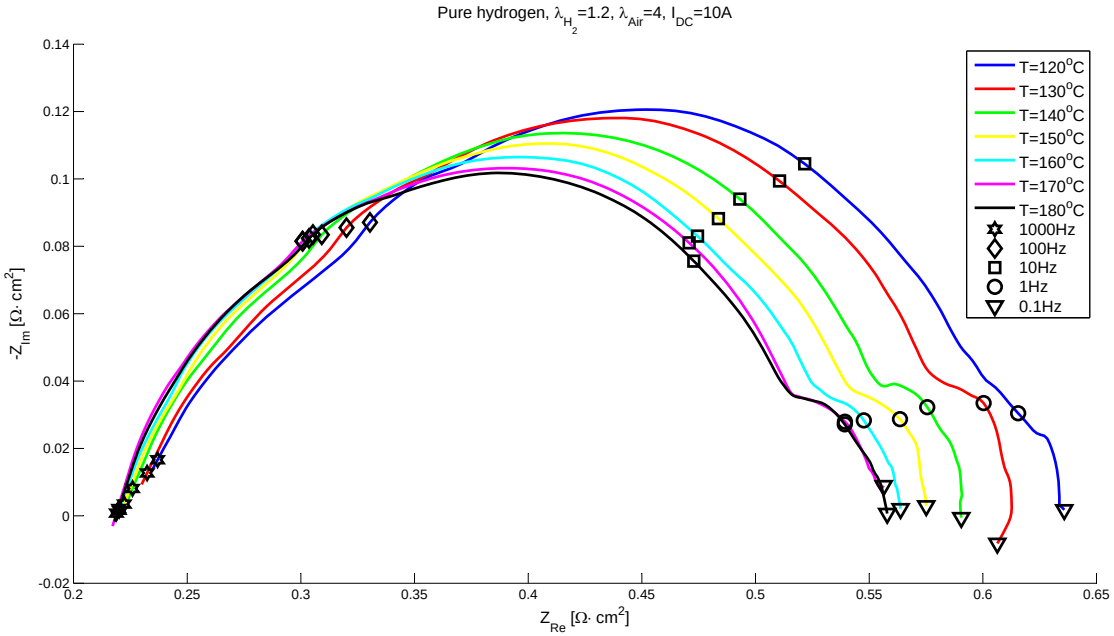

Figure 2: Nyquist plot of the HTPEM fuel cell impedance at I_{DC}=10A, on pure hydrogen at different temperatures.

The shown impedance can be analyzed using different modeling approaches an equivalent electrical circuit model can be found for system simulations of the fuel cell, or other aspects of fuel cell performance can be analyzed.

3. Experimental setup

For examining the fuel cell under test, an experimental setup is used, where a single cell assembly consisting of a BASF P2100 fuel cell mounted between two PTFE gaskets, carbon composite flow plates all clamped together by stainless steel endplates with cartridge heaters for keeping a constant fuel cell temperature during operation. The assembly is shown in figure 3. The anode gas is supplied by three Bürkert 8711 mass flow controllers (MFC), enabling the introduction of different concentrations of H_2, CO and CO_2, all typical components in fuel cells fuelled by reformers. The cathode side is in a similar way controlled by a Bürkert 8712 MFC supplied by compressed air. The data acquisition, control and automation of the different tests conducted by a Labview virtual interface and three National Instruments PCI units, NI PCI 6229, NI PCI 4351 and NI PCI 6704

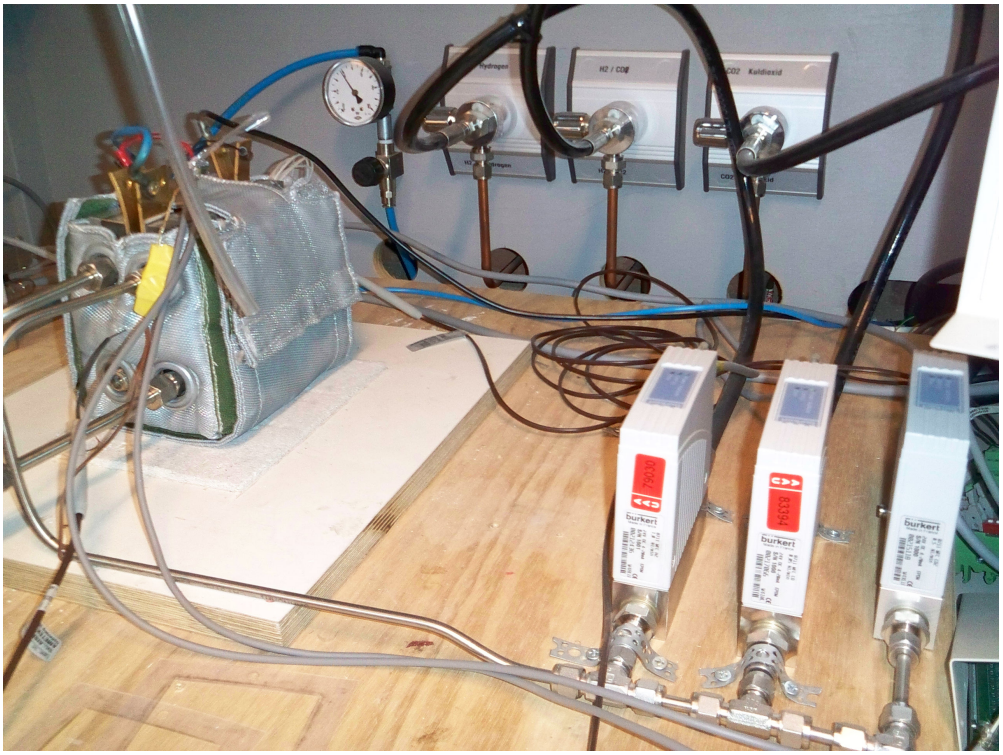

Figure 3: Picture of the test setup.

The current drawn from the fuel cell is effectuated by a 800W TDI Power RBL488 50-150-800 electronic load, and an additional Labview based system, using a PCI 6259 is used to conduct the impedance measurements. The settings for the impedance system when measuring the full impedance spectrum is as follows:

- Frequency range 1kHz to 0.1Hz
- Max current amplitude 3A
- 25 frequencies per logarithmic decade

The CO estimation algorithm is implemented in the Labview impedance measurement systems and provided with three input measurements needed as for the CO estimation algorithm. These are current $i_{cell}(t)$, voltage $V_{cell}(t)$ and temperature $T_{cell}(t)$.

4. CO estimator algorithms

The CO estimator algorithm use one frequency, at which impedance measurements are done at varying CO, CO_2 $i_{cell}(t)$ and temperature ($T_{cell}(t)$). The measurements are then mapped by a surface defined by polynomials. The available variables for the mapping are the CO value, the temperature and the real and imaginary parts of the impedance. The CO value is an output and therefore always used, whereas the other inputs can be chosen as a combination of the other variables.

The polynomial fits are done for measurements with $i_{cell}(t)$ at the range 10 to 17.5$[A]$, $T_{cell}(t)$ in the range 155 to 175$[°C]$ and CO_2 in the range 0 to 30$[\%]$. The constant frequency is set at 105$[Hz]$, which was placed in the middle of the desired range of interest between 100 and 110$[Hz]$, which isn't too slow to be uncertain, due to changing system states such as temperature and gas concentrations, but neither to fast to require fast electronics. If the fuel cell system is delivering power to a 50 Hz grid through a single phase inverter the frequency of the dc-link voltage will be twice of the grid frequency, i.e. 100 Hz. This means that by designing the dc-link capacitor properly in order to have an appropriate dc-link voltage ripple the CO-concentration can be estimated from the inherent small ac-signal of the inverter. It is therefore not necessary to have any additional hardware in order to superimpose an ac-signal in the fuel cell current. However, analyzing the impedance due to a single phase grid-inverter is left for future work as the purpose for this paper is to demonstrate the relationship between the CO-concentration, temperature and impedance.

The fit results are illustrated in the following three figures 4, 5 and 6, which show both the shape of the fits and their residuals.

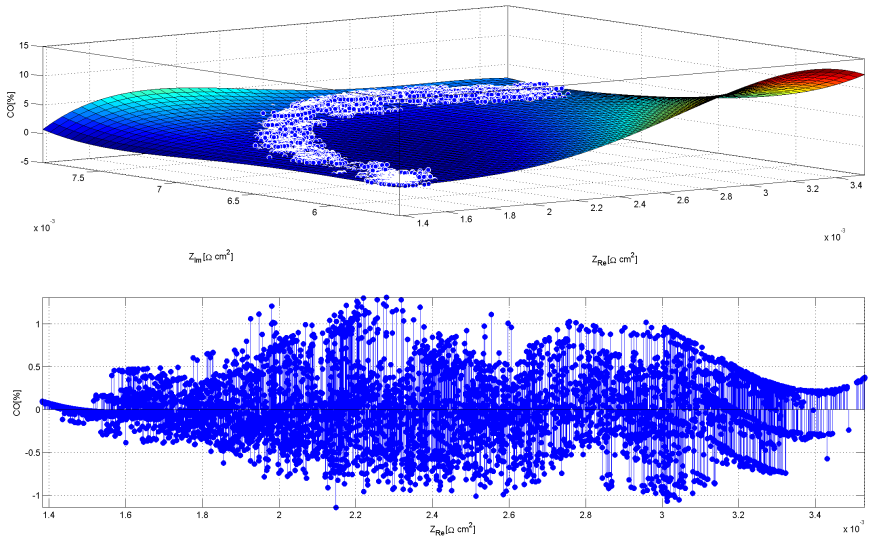

Figure 4: Design of the 1st CO estimator, with the inputs: $Z_{Re}(t)$ and $Z_{Im}(t)$.

The algorithms defining the mappings to CO are derived using polynomials of the order 4 and 4, which has the following form:

$$\begin{aligned} CO_{est}(t)[\%] = {} & p_{00} + p_{10}x(t) + p_{01}y(t) + p_{20}x(t)^2 + p_{11}x(t)y(t) + p_{02}y^2 + p_{30}x(t)^3 + p_{21}x(t)^2y(t) + p_{12}x(t)y(t)^2 \\ & + p_{03}y(t)^3 + p_{40}x(t)^4 + p_{31}x(t)^3y(t) + p_{22}x(t)^2y(t)^2 + p_{13}x(t)y(t)^3 + p_{04}y(t)^4 \end{aligned} \quad (3)$$

, where the inputs and constants are specific for each CO estimator number:

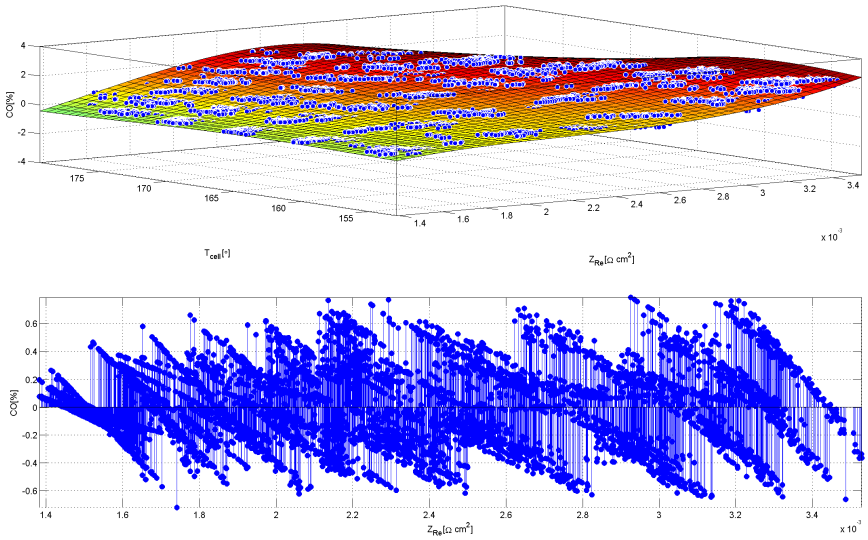

Figure 5: Design of the 2nd CO estimator, with the inputs: $Z_{Re}(t)$ and $T_{cell}(t)$.

1. $x(t)$ is the real part of the impedance measurement ($Z_{Re}(t)$), $y(t)$ is the imaginary part of the impedance measurement ($Z_{Im}(t)$) and the constants are:
   p_{00} = 974.86998357924824, p_{10} = 355652.89198044885, p_{01} = -719017.06812596519
   p_{20} = 13651868.496985577, p_{11} = -164331357.03022113, p_{02} = 192603361.51394019
   p_{30} = 8923826118.2576504, p_{21} = -10405152921.542259, p_{12} = 26737014581.621918
   p_{03} = -22524744938.23312, p_{40} = -3856269810854.4072, p_{31} = 4235101263284.8267
   p_{22} = -1634213550500.0017, p_{13} = -874591099518.78516, p_{04} = 927327446188.15051
2. $x(t)$ is the real part of the impedance measurement ($Z_{Re}(t)$), $y(t)$ is the temperature measurement ($T_{cell}(t)$) and the constants are:
   p_{00} = 1787.6150832153778, p_{10} = 1463318.473086644, p_{01} =-58.795638262515595
   p_{20} = -278784271.84294492, p_{11} = -20257.273369942086, p_{02} = 0.63971065306233743
   p_{30} = 15592241318.218281, p_{21} = 2863913.5993069424, p_{12} = 89.318472127976719
   p_{03} = -0.0028821293407541378, p_{40} = -55260546104.019379, p_{31} = -93627348.27086834
   p_{22} = -7093.0558676384117, p_{13} = -0.12320688595788029, p_{04} = 4.646738529168038e-6
3. $x(t)$ is the imaginary part of the impedance measurement ($Z_{Im}(t)$), $y(t)$ is the temperature measurement ($T_{cell}(t)$) and the constants are:
   p_{00} = -5480.7538313315272, p_{10} = 1002880.7779525866, p_{01} = 91.432572873854767
   p_{20} = -124845012.19590963, p_{11} = -7736.6653833052951, p_{02} = -0.6699016704172126
   p_{30} = 3629480091.6688304, p_{21} = 1055462.7823221444, p_{12} = 2.1462557021521174
   p_{03} = 0.0026690942152858481, p_{40} = -258675025328.43097, p_{31} = 20611436.140699334
   p_{22} = -4403.4762059475961, p_{13} = 0.11716504040925634 , p_{04} = -5.2164030092854899e-6

4.1. Preliminary analysis of the algorithms

The polynomial fit errors are presented in table 1.

The algorithms can be analysed in three ways. The first is the errors from table 1, which shows that the polynomial with the $Z_{Re}(t)$ and $T_{cell}(t)$ inputs is the best by at least 35%. It is followed by the polynomial with the $Z_{Re}(t)$ and $Z_{Im}(t)$ inputs, which is an improvement by around 12% over the last polynomial fit.

The second way to analyse the polynomial fits is with the figures. The polynomial with the $Z_{Re}(t)$ and $Z_{Im}(t)$ inputs have inputs that are clustered in an arc, which is expected from impedance results, but as they don't span the whole

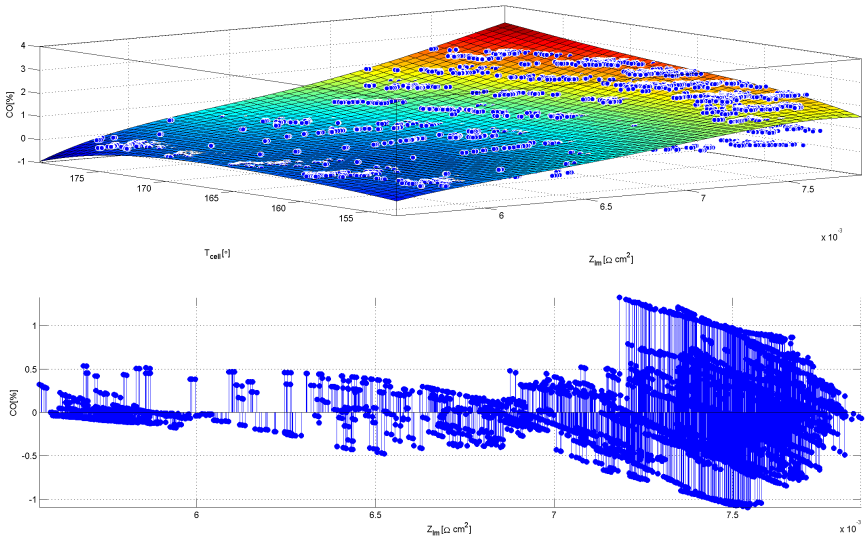

Figure 6: Design of the 3rd CO estimator, with the inputs: $Z_{Im}(t)$ and $T_{cell}(t)$.

CO Estimator #	Input Variables		Fit Results		
	1st	2nd	R^2	Adjusted R^2	RMSE
1	$Z_{Re}(t)$	$Z_{Im}(t)$	0.8001512083869896	0.7996319279336521	0.38253441530318866
2	$Z_{Re}(t)$	$T_{cell}(t)$	0.8908355506039385	0.8905519013293385	0.28272249462613563
3	$Z_{Im}(t)$	$T_{cell}(t)$	0.7487133659915381	0.7480604311592964	0.428947799657735

Table 1: Table for polynomial plane error values.

surface and just a part of it, then there is less robustness in the mapped plane. This translates a higher uncertainty, when the system ages. The other two polynomials span the mapped plane nicely and are therefore expected to have better robustness.

The third way to analyse the polynomials is by evaluating their constants. Again the polynomial with the $Z_{Re}(t)$ and $Z_{Im}(t)$ inputs stand out with larger higher order constants than the other two. This is also visible in the figures of the polynomials as the mapped surface reach higher CO values than the other two polynomials by a factor of at least 300%. This indicates less robustness for the polynomial with the $Z_{Re}(t)$ and $Z_{Im}(t)$ inputs, but it doesn't guarantee it.

5. Experimental results

The polynomial fits are designed for measurements done with $i_{cell}(t)$ in the range 10 to 17.5$[A]$, $T_{cell}(t)$ in the range 155 to 175$[°C]$ and CO_2 in the range 0 to 30%, while the tests are done in almost the same range, though with the extension of $T_{cell}(t)$ in the range 155 to 180$[°C]$. The algorithms aren't designed for 180$[°C]$, but this was included to show robustness outside the operating range.

The following subsections are comprised of test results with or without filtering, where the first subsection contains the results obtained without filtering, while the second subsection contains the results with the filtering.

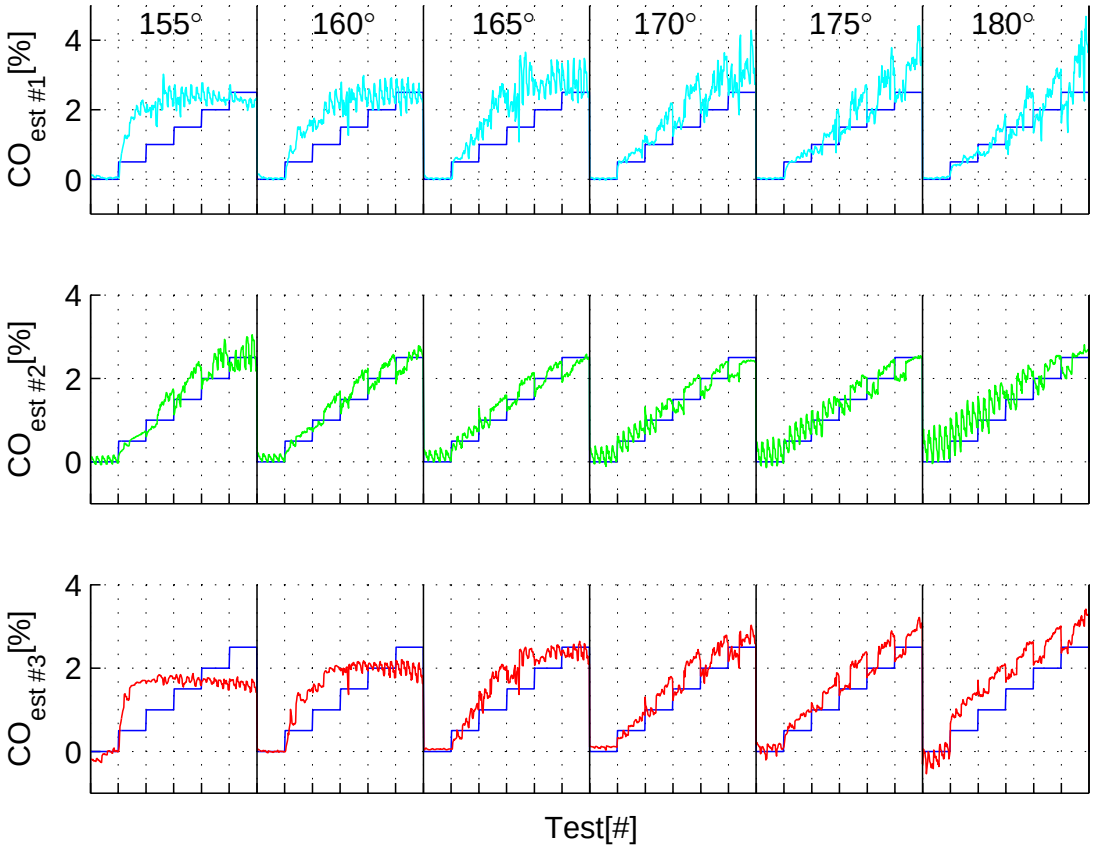

Figure 7: Plot unfiltered.

5.1. Verification test

The figure 7 illustrates the test results of the CO estimators. The shapes of the first and third CO estimators are comparable, as they both have problems estimating at the lower temperatures where zero is estimated acceptable, but any other CO value results the same estimate. When the temperature rises, then they both also start following the CO value. The second CO estimator differs as this seem to follow the CO value for any temperature.

The third CO estimator has a good tracking performance in the temperature range $170 - 175[^{\circ}C]$, and a decent tracking performance (Error is less than 1.5[%]). While the first has a decent tracking performance (Error is around than 2[%]). The second CO estimator also show relation to the temperature, as $i_{cell}(t)$ has a higher influence on the precision at higher temperature.

5.2. Filtered verification test

The mean filtered tests results presented in figure 9 have a smaller variation than the unfiltered results in figure 7. The offset of the filtered tests follow the same characteristics and shape as for the unfiltered tests. Hence the jitter shown in the results aren't pure white noise. Furthermore, the carry frequency of the noise is the same frequency as the changes in the test parameters.

The difference between the error plots for the filtered and non-filtered test results are small, but the is one notible and that is for the second CO estimator at 180[°] and 0% CO in the fuel. Here the filter actually increase the error.

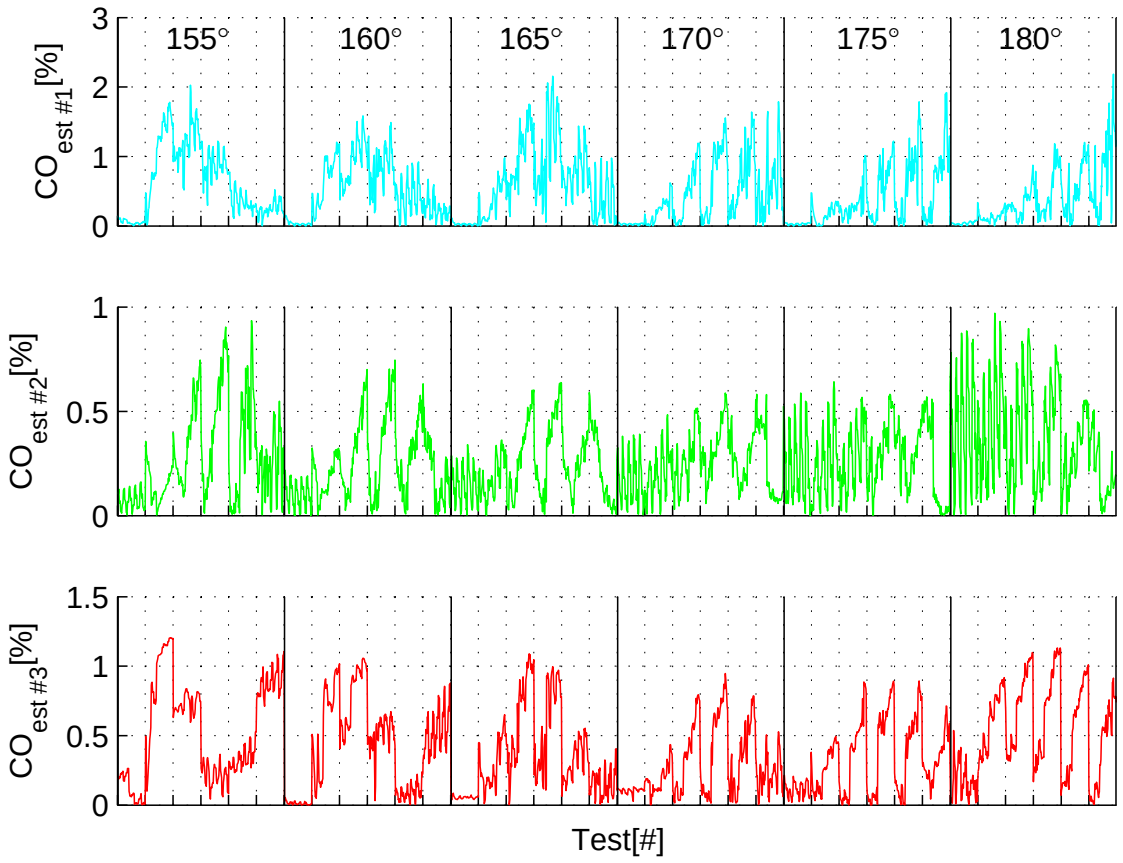

Figure 8: Unfiltered error between estimate and real value.

6. Conclusion

The figure 7 illustrates the CO estimators 1 and 3 both fail to follow the CO value at lower temperatures, while there is no such problem with the second CO estimator. This indicate a strong relation between $Z_{Re}(t)$, $T_{cell}(t)$, and CO concentration.

The presented CO estimators delivers acceptable results, but there are differences between their performance. There isn't one algorithm that is better than others for all situations, but there is one that overall has better performance and that is the second CO estimator, which provides acceptable results in most situations, but is surpassed at lower CO values.

The first CO estimator provides good CO estimation at 0%, and lower CO values at increasing temperatures. This however doesn't stop the CO estimator from giving the worst estimations at the other end.

The main improvement in the presented paper is the runtime CO estimation methods, which prove promising results. The other alternatives at the present time are either a gas analyser, as known CO sensors are cross gas sensitive, or methods under research, e.g. impedance spectroscopy.

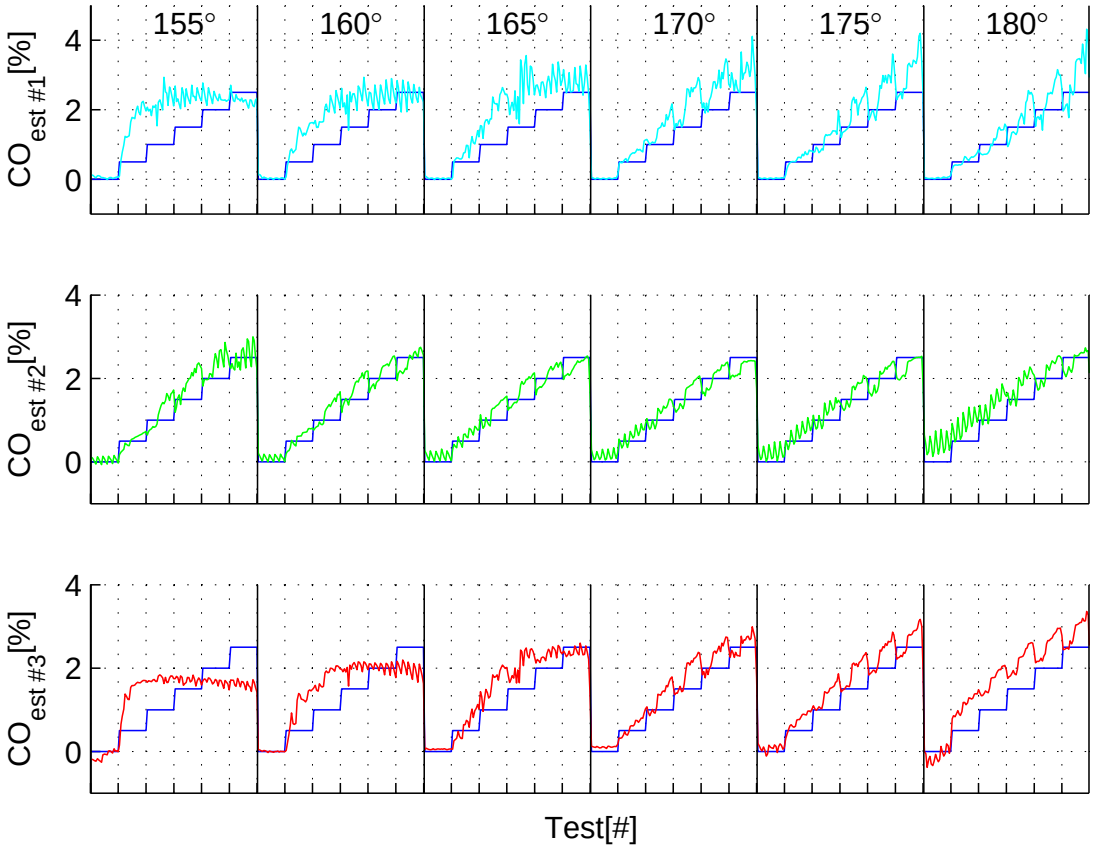

Figure 9: Plot mean filtered with a filter length of 3 samples.

7. Future work

The next step is to implement the approach on a different setup with either a reformer or a fuel cell stack. A experimental setup with a reformer can be used to test the desired improved performance, which should come with the knowledge about CO contents. Whereas a setup with a fuel cell stack rather than a experimental setup would prove the functionality of the approach on a real setup with appropriate measurement values and noise.

Appendix

The results are presented in the following table. The table .2 contains the largest deviation obtained with the filtered results for all the CO estimators. The following three tables (.3,.4 and .5) has the filtered results for all the CO estimators in higher detail.

Andreasen, S. J., Kær, S. K., Nielsen, M. P., 2008. Experimental evaluation of a pt-based heat exchanger methanol reformer for a HTPEM fuel cell stack. Electrochemical Society Transactions 12, 571–578.

Andreasen, S. J., Vang, J. R., Kær, S. K., 2011. High temperature pem fuel cell performance characterisation with co and co2 using electrochemical impedance spectroscopy. International Journal of Hydrogen Energy 36, 9815–9830.

Avgouropoulos, G., Papavasiliou, J., Daletou, M. K., Kallitsis, J. K., Ioannides, T., Neophytides, S., 2009. Reforming methanol to electricity in a high temperature pem fuel cell. Applied Catalysis B: Environmental Issues 3-4 90, 628–632.

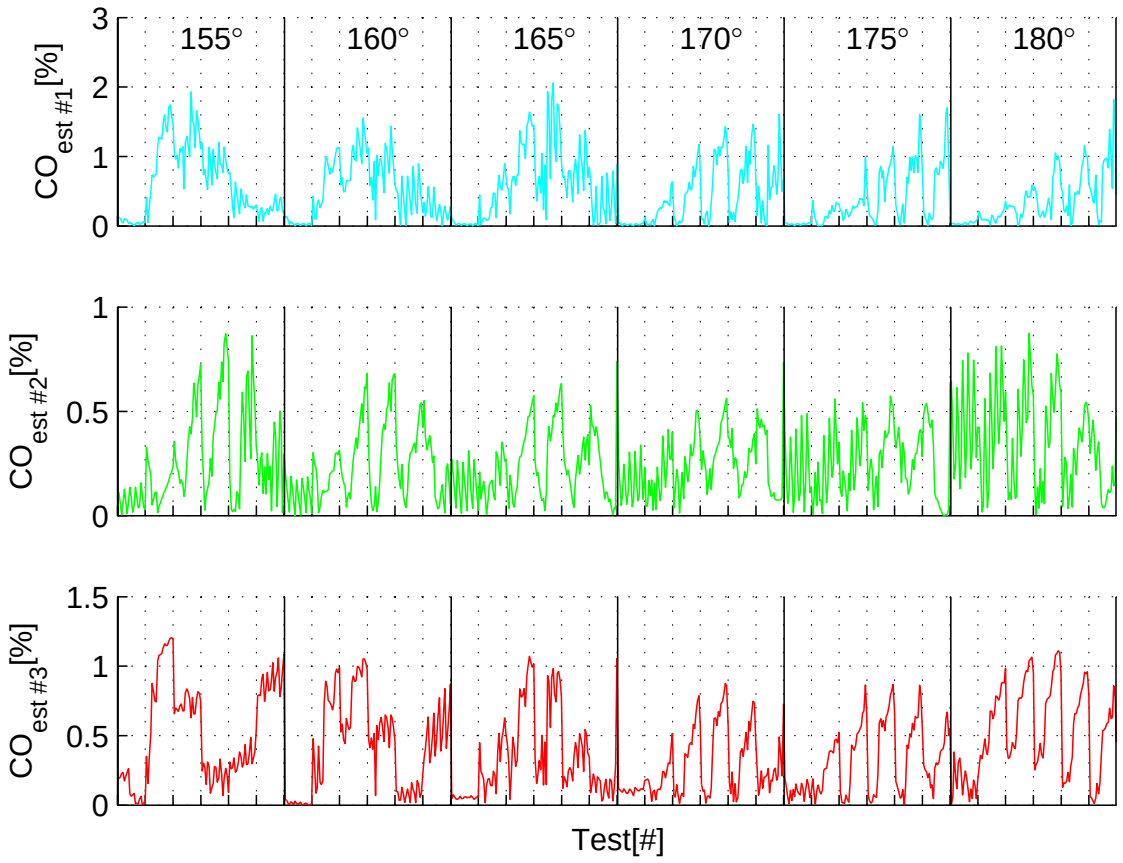

Figure 10: Filtered error between estimate and real value. Filter length of 3 samples.

CO Estimator	Input		$T_{cell}(t)$					
	1st	2nd	155°	160°	165°	170°	175°	180°
# 1	$Z_{Re}(t)$	$Z_{Im}(t)$	1.9315	1.5522	2.0603	1.6110	1.7023	1.8220
# 2	$Z_{Re}(t)$	$T_{cell}(t)$	0.8717	0.6804	0.7385	0.7340	0.6371	0.8730
# 3	$Z_{Im}(t)$	$T_{cell}(t)$	1.2037	1.0512	1.0703	0.8757	0.8687	1.1114

Table .2: Table of maximum error values obtained in verification test with the *CO* estimators.

BASF, 2011a. 6546 produktblatt celtecmeas 2 ansicht.
URL http://www.fuel-cell.basf.com/ca/internet/Fuel_Cell/en_GB/function/conversions:/publish/content/Microsite/Fuel_Cell/6546_Produktblatt_CeltecMEAs_2_Ansicht.pdf
BASF, 2011b. Basf fuel cell.
URL http://www.fuel-cell.basf.com/ca/internet/Fuel_Cell/
Choudhury, S. R., Rengaswamy, R., 2006. Characterization and fault diagnosis of pafc cathode by eis technique and a novel mathematical model approach. Journal of Power Sources 161, 971986.
DOE, 2011.
URL http://www1.eere.energy.gov/hydrogenandfuelcells/pdfs/accomplishments.pdf
Fouquet, N., Doulet, C., Nouillant, C., Dauphin-Tanguy, G., Ould-Bouamama, B., 2006. Model based pem fuel cell state-of-health monitoring via

	CO					
$T_{cell}(t)$	0[%]	0.5[%]	1[%]	1.5[%]	2[%]	2.5[%]
155°	0.1259	1.7426	1.9315	1.2058	0.7729	0.4566
160°	0.1371	1.1294	1.5522	1.4369	0.8951	0.5645
165°	0.1099	0.8948	1.6409	2.0603	1.3752	0.8816
170°	0.1238	0.6347	1.1717	1.4251	1.4629	1.6110
175°	0.0449	0.3716	0.9793	1.1455	1.6068	1.7023
180°	0.1089	0.3551	0.5870	1.0503	1.1569	1.8220

Table .3: Table of maximum error values obtained in verification test with 1st CO estimator (Inputs: $Z_{Re}(t)$ and $Z_{Im}(t)$).

	CO					
$T_{cell}(t)$	0[%]	0.5[%]	1[%]	1.5[%]	2[%]	2.5[%]
155°	0.1578	0.3272	0.7240	0.8717	0.8623	0.5004
160°	0.2086	0.3131	0.6804	0.6790	0.5407	0.5505
165°	0.3110	0.3529	0.5759	0.6334	0.3916	0.7385
170°	0.3381	0.4123	0.5045	0.5622	0.4184	0.7340
175°	0.4884	0.5598	0.5411	0.5728	0.4239	0.6371
180°	0.7792	0.8129	0.8730	0.7754	0.5417	0.4570

Table .4: Table of maximum error values obtained in verification test with 2nd CO estimator (Inputs: $Z_{Re}(t)$ and $T_{cell}(t)$).

	CO					
$T_{cell}(t)$	0[%]	0.5[%]	1[%]	1.5[%]	2[%]	2.5[%]
155°	0.2622	1.2037	0.8363	0.3305	0.5248	1.0876
160°	0.0393	0.9891	1.0512	0.6490	0.2276	0.8697
165°	0.0744	0.6262	1.0703	0.9819	0.5445	1.0545
170°	0.1767	0.5149	0.7860	0.8757	0.7459	0.7256
175°	0.1933	0.5228	0.8644	0.8687	0.8625	0.6684
180°	0.3823	0.9847	1.0652	1.1114	0.9603	0.8577

Table .5: Table of maximum error values obtained in verification test with the 3rd CO estimator (Inputs: $Z_{Im}(t)$ and $T_{cell}(t)$).

ac impedance measurements. Journal of Power Sources 159, 905913.

Gebregergis, A., Pillay, P., Rengaswamy, R., 2010. Pemfc fault diagnosis, modeling, and mitigation. IEEE Transactions on Industry Applications, NO. 1, JANUARY/FEBRUARY 46, 295–303.

http://www.fuelcells.org/info/charts/h2fuelingstations.pdf, 2012. Worldwide hydrogen fueling stations. Tech. rep., http://www.fuelcells.org.

http://www.hydrogen.energy.gov/pdfs/review10/st001_ahluwalia_2010_o_web.pdf, 2010. System level analysis of hydrogen storage options. Tech. rep., Argonne National Laboratory.

Jensen, J. O., Li, Q., Pan, C., Vestb, A. P., Mortensen, K., Petersen, H. N., Srensen, C. L., Clausen, T. N., Schramm, J., Bjerrum, N. J., 2007. High temperature pemfc and the possible utilization of the excess heat for fuel processing. International Journal of Hydrogen Energy, Issues 10-11 32, 1567–1571.

Kolb, G., Keller, S., Tiemann, D., Schelhaas, K.-P., Schrer, J., Wiborg, O., 2012. Design and operation of a compact microchannel 5 kwel,net methanol steam reformer with novel pt/in2o3 catalyst for fuel cell applications. Chemical Engineering Journal,Issues 1-2 207-208, 388–402.

Li, Q., Jensen, J. O., Savinell, R. F., Bjerrum, N. J., 2009. High temperature proton exchange membranes based on polybenzimidazoles for fuel cells. Progress in Polymer Science 34, 449–477.

Merida, W., Harrington, D., Canut, J. L., McLean, G., 2006. Characterisation of proton exchange membrane fuel cell (pemfc) failures via electrochemical impedance spectroscopy. Journal of Power Sources 161, 264274.

Pehnt, M., 2001. Life-cycle assessment of fuel cell stacks. International Journal of Hydrogen Energy 26, 91–101.

Tian, G., Wasterlain, S., Candusso, D., Harel, F., Hissel, D., Francois, X., 2010. Identification of failed cells inside pemfc stacks in two cases: Anode/cathode crossover and anode/cooling compartment leak. International Journal of Hydrogen Energy 35, 2772–2776.

Yuan, X., Wang, H., Sun, J. C., Zhang, J., 2007. Ac impedance technique in pem fuel cell diagnosis – a review. International Journal of Hydrogen Energy 32 (17), 4365 – 4380.

Zhang, J., Xie, Z., Zhang, J., Tang, Y., Songa, C., Navessin, T., Shi, Z., Songa, D., Wang, H., Wilkinson, D. P., Liu, Z.-S., Holdcroft, S., 2006. High temperature pem fuel cells. Journal of Power Sources 160, 872–891.